SUPPLEMENT TO THE *WELDING JOURNAL*, JANUARY 2009
Sponsored by the American Welding Society and the Welding Research Council

A CCT Diagram for an Offshore Pipeline Steel of X70 Type

The diagram developed is valid for the heat-affected zone for welding operations where relatively rapid heating up to 1200°C occurs

BY M. I. ONSØIEN, M. M'HAMDI, AND A. MO

ABSTRACT

By means of dilatometry and metallographic analyses, a continuous-cooling transformation (CCT) diagram valid for the heat-affected zone (HAZ) in welding operations with relatively rapid heating up to about 1200°C on an offshore pipeline steel of X70 type has been established along with the linear thermal expansion coefficients for the austenite and bainite phases. A dilatometer was built for this purpose. For comparison reasons, the steel was also tested in a commercial dilatometer using larger samples than in the laboratory-built dilatometer. The importance of using relatively small dilatometry samples in order to minimize the inaccuracy associated with the temperature gradients has been substantiated by means of mathematical modeling showing that cylindrical samples of 20-mm length and 3-mm diameter are sufficiently small.

Introduction

Modeling of stresses and deformations induced during welding of phase-transforming steels requires constitutive equations quantifying the flow stress during the viscoplastic deformation of the material. The establishment of such equations is demanding as a series of complex phenomena should be accounted for, such as work hardening, strain rate sensitivity, and the flow stress dependency on the specific mixture of phases appearing at the different temperatures. The phase transformations per se also lead to so-called transformation plasticity when stresses are applied, and the volumetric strains associated with the transformations along with the thermal strains constitute the driving force for the stress/deformation development. Additional scientific challenges have to be dealt with when the equation parameters are to be experimentally determined.

The complexity in developing reliable constitutive equations for welding stress and deformation in steels indicates a need for simplified approaches. Indeed, constitutive equations applied in most engineering models today are relatively simple (Refs. 1–4) and often based on the ideal plasticity assumption, taking the flow stress of each phase to be given by the temperature-dependent yield stress for that phase in combination with a mixture law (Ref. 2). A new approach in accordance with these ideas was recently presented along with the determination of the temperature- and microstructure-dependent flow stress for a pipeline steel of X70 type (Ref. 5). This approach requires prior knowledge of the relevant continuous-cooling-transformation (CCT) diagram providing information about the involved phases and the temperatures at which the phase transformations take place during continuous cooling.

Continuous-cooling-transformation diagrams can be established by means of dilatometry experiments (Refs. 6–11) in which the volume expansion/contraction associated with temperature changes and phase transformations are quantified. Such an experiment reveals how the length change of an unloaded specimen varies with temperature, and this is usually quantified by means of a dilatometry curve similar to that shown schematically in Fig. 1. For ferritic steels, the upper and lower straight lines correspond typically to pure ferrite and austenite phases with slopes equal to the respective linear thermal expansion coefficients. The transformations between the phases, during which the phases coexist, are furthermore reflected in the nonlinear parts of the dilatometry curves.

The purpose of the present article is to report the establishment of a CCT diagram valid for the heat-affected zone (HAZ) in welding operations with relatively rapid heating up to about 1200°C of the offshore X70 pipeline steel with the composition given in Table 1. This diagram has, to the knowledge of the authors, not been reported elsewhere in the open scientific literature. Hulka et al. (Ref. 12) has published similar X70 data; however, the chemical composition in their investigated steel was different from that in Table 1. This difference influences significantly the microstructure and hardenability.

In order to obtain small temperature gradients in the samples, a new dilatometer was built, and for comparison reasons, the steel was also tested in a commercial dilatometer (Ref. 13) using larger samples than in our laboratory-built dilatometer. The experimental procedures are outlined in the following section. The results, including metallographic examination of the samples, are presented and discussed later along with a presentation of the final CCT diagram.

KEYWORDS

Continuous Cooling Transformation Diagrams
Dilatometry
Heat-Affected Zone
Phase Transformations
Pipeline Steels

M. I. ONSØIEN, M. M'HAMDI, and A. MO are with SINTEF, Trondheim, Norway.

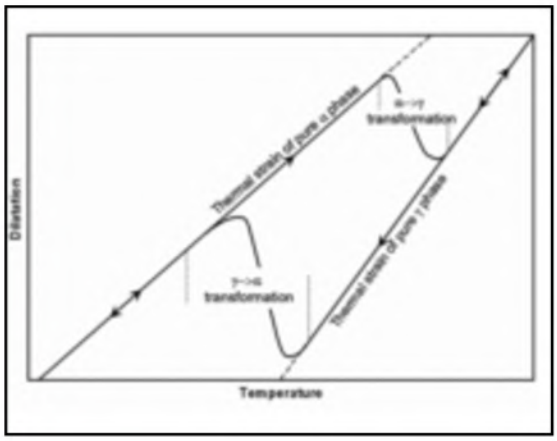

Fig. 1 — Schematic dilatometry diagram of a ferritic steel.

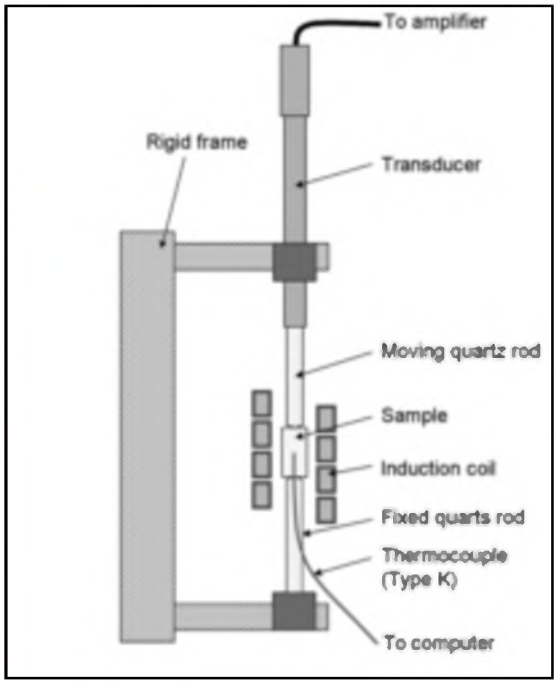

Fig. 2 — Schematic drawing of the laboratory-built dilatometer.

Experimental Procedures

For the laboratory-built dilatometer, cylindrical samples of 20-mm length were machined from the API 5L X70 (Ref. 14) pipeline base metal. Two sets, having diameters of 3 and 10 mm, respectively, were made with the purpose of studying how different geometries would respond to the rapid heating and cooling cycles and thus affect the measurements. The samples for the commercial dilatometer were 65 mm long and had a 10 × 10 mm^2 cross section. All samples were machined such that the dilatometry measurements were carried out in the longitudinal direction of the pipe.

Experimental Setup and Testing

A schematic drawing of the laboratory-built dilatometer is shown in Fig. 2. It consists of a displacement transducer mounted in a rigid frame, and the sample is mounted between two quartz rods, one moving and one fixed. A spring-loaded moving quartz rod is connected to the transducer. Heating of the sample is provided by means of an induction coil, while cooling of the specimen is accomplished by flushing the sample with helium and/or argon. The temperature was recorded by a Type K thermocouple, with wire diameter of 0.5 mm, spot welded to the sample surface at mid-length. Upon heating/cooling, the sample expands/contracts and pushes on the quartz rods. This movement was captured by the displacement transducer and recorded by the computer. The sensitivity of the dilatation measurements is, based on data given by the displacement transducer manufacturer (Ref. 15), estimated to correspond to a fraction transformed of about ± 3.1%.

In the commercial dilatometer (Ref. 13), the sample is mounted in water-cooled copper clamps and heated by the Joule effect. Controlled cooling is accomplished by reducing the electric current such that there is a net heat flux from the sample to the cold copper clamps. The dimensional changes were measured over the cross section of the sample, limited to a gauge length of around 10 mm.

The samples, both for the laboratory-built and the commercial dilatometer, were subjected to thermal cycles similar to those in welding operations of rapid heating (150°C/s) to a peak temperature, T_p, of 1200°C prior to cooling. The cooling times between 500° and 800°C, $\Delta t_{8/5}$, were about 5, 10, 20, and 100 s. Dilatometry curves similar to the one schematically shown in Fig. 1 were established for each sample geometry and cooling time. Extractions of transformation start and finish temperatures from the dilatation curves were done manually. An estimated accuracy of ± 5°C in the manual determination of transformation start and end temperatures is expected based on the following procedure. A baseline was drawn on top of the linear portion of the dilatation curves from approximately 100°C above the transformation start. The transformation start temperature was found where the dilatation curve starts to deviate from this baseline. Similarly the transformation finish temperature was found by means of the baseline drawn from approximately 100°C below the transformation finish temperature. This procedure is schematically illustrated in Fig. 3. For the most rapid cooling time, i.e., $\Delta t_{8/5}$ of 1.4 s, the transformation temperatures were determined by derivation of the cooling curve, since the dilatation curve in this case was too rugged.

Continuous-cooling-transformation diagram data were obtained over about two orders of magnitude in cooling time ($\Delta t_{8/5}$), also the linear thermal expansion coefficients of the high- and low-temperature phases, austenite and bainite, respectively, were determined from the dilatometry curves during cooling.

Microstructure and Temperature Gradients in the Samples

The metallographic samples were ground to a 1000-grit finish and polished using 3- and 1-μm diamond spray prior to etching in a 2 vol-% nital solution to reveal the microstructure. The microstructure of the base metal and of the samples after the dilatometry tests was characterized by means of light microscope point counting. For each sample, at least 1000 points were counted at a magnification of 500× using a 10 by 10 grid in the microscope. The microstructure constituents were classified as martensite (M), upper bainite, lower bainite and acicular ferrite (B), grain boundary or polygonal ferrite (F), and pearlite (P), where the letters in parentheses are the usual symbols that in the present article are used in Table 2. The metallographic examination also included measurements of Vickers hardness (HV_{10}).

The relatively high heating and cooling rates imposed by the induction heating and gas cooling lead to temperature gradients in the radial sample direction. The heat transfer in the 3- and 10-mm-diameter axisymmetric samples was, therefore, quantified by means of the FEM software *WeldsimS* (Ref. 16). Brief descriptions of the governing equations, phase transformation model as well as geometries and boundary conditions employed in the simulations with *WeldsimS* are all given in the Appendix. In the simulations, the fastest measured surface cooling curve for the 10-

Table 1 — Chemical Composition of the X70 Pipeline Steel (elements in wt-%)

C	Si	Mn	P	S	Cr	Ni	Al	Cu	Mo	Nb	V	Ti	N
0.09	0.30	1.71	0.012	0.001	0.07	0.05	0.05	0.04	0.02	0.05	0.01	0.02	0.005

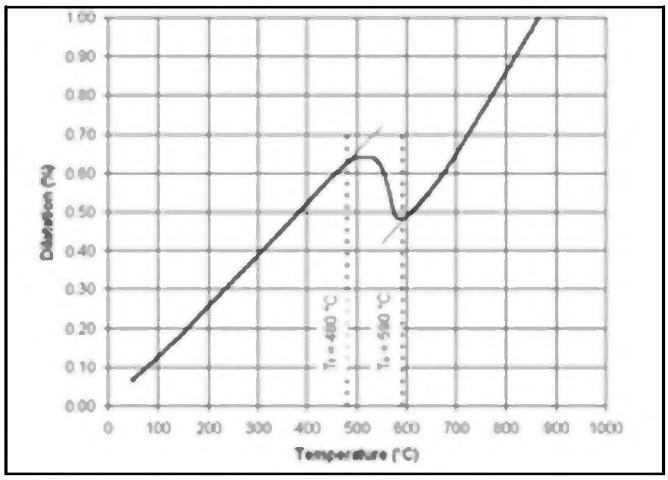

Fig. 3 — Illustration of procedure for manual transformation temperature determination from dilatation curve acquired from 3-mm-diameter sample with $\Delta t_{8/5}$=23.5 s.

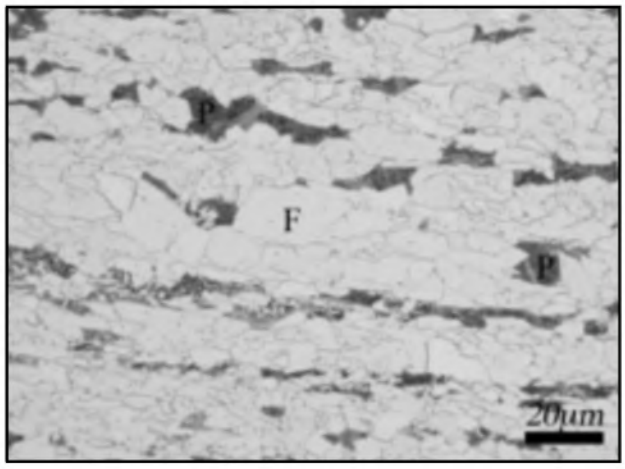

Fig. 4 — Microstructure in the base metal.

mm-diameter samples was imposed as boundary condition, i.e., a thermal cycle with T_p = 1200°C and $\Delta t_{8/5}$ = 5.5 s.

Results and Discussion

Experimental Results

The initial microstructure of the base metal shown in Fig. 4 consisted of mainly ferrite (86%) with bands of pearlite (14%). The average hardness was 200 HV_{10}.

Altogether 11 dilatometry curves were established, and typical results obtained in the laboratory-built and commercial dilatometer are shown in Fig. 5. Note that dilatometry curves were obtained only during cooling in the laboratory-built dilatometer since the transducer was strongly affected by noise from the induction coil used during heating. This means that the phase boundaries upon heating, i.e., A_{c1} and A_{c3}, were determined solely on the basis of the commercial dilatometer tests.

The results from the dilatometry measurements are summarized in Table 2. In all cases, the austenite decomposition resulted in the formation of bainite and/or martensite, and the transformation from austenite to bainite is shifted toward lower temperatures as $\Delta t_{8/5}$ is decreased. Typical microstructures are shown in Fig. 6

For the highest values of $\Delta t_{8/5}$ (> 20 s), the transformation product is bainite. Even the highest cooling times, $\Delta t_{8/5}$ = 107.2 and 109.4 s, resulted in a fully bainitic microstructure, as evidenced for $\Delta t_{8/5}$ = 107.2 s by the micrograph in Fig. 7. This result is somewhat unexpected since microstructure constituents such as grain boundary ferrite or polygonal ferrite are more usual at this high $\Delta t_{8/5}$ (Ref. 17). The observation is, however, in agreement with similar findings reported by Hulka et al. (Ref. 12). For the lower values of $\Delta t_{8/5}$ (< 10 s), martensite is formed in addition to bainite. As expected, the increase in martensite fraction for decreasing $\Delta t_{8/5}$ is accompanied by an increase in the hardness (Ref. 18).

The martensite transformation start temperature, denoted by M_s, as well as the A_{c1} and A_{c3} temperatures were finally determined. While the determination of M_s was based on 3-mm-diameter samples, A_{c1} and A_{c3} were determined on the basis of the square samples using the commercial equipment. The results were M_s = 437°C, A_{c1} = 760°C, and A_{c3} = 920°C. The experimentally determined value of M_s is close to that calculated by the empirical formulas in Ref. 19 to be 444°C.

The average linear thermal expansion coefficients were determined from the dilatometry curves, during cooling, to 2.09×10^{-5} and 1.29×10^{-5} K^{-1} for the austenite and bainite phases, respectively. These values are close to data reported by Takahashi (Ref. 20).

The CCT Diagram

The CCT diagram shown in Fig. 8 was established on the basis of all dilatometry and metallography data summarized in Table 2, which includes all three sample geometries and the use of both the laboratory-built and the commercial dilatometer. The diagram reveals that the cooling rate dependent onset temperature for the phase transformation occurs at about the same temperature for all three sample geometries. The temperatures at which the transformation is finished is, however, lower for the larger samples; the difference being about 30°C between the 10-mm- and 3-mm-diameter samples when $\Delta t_{8/5}$ is about 5 s.

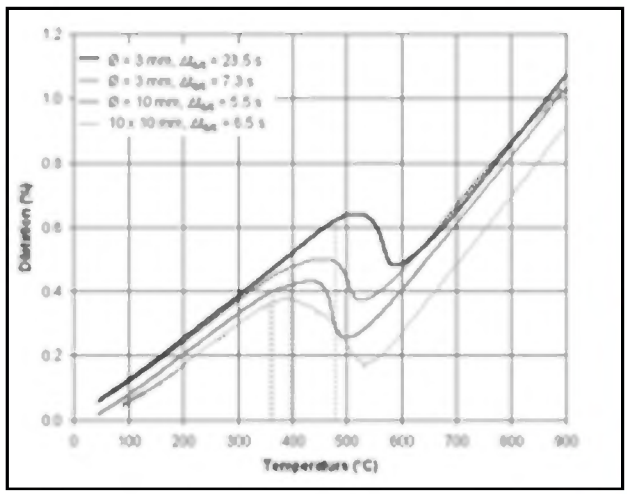

Fig. 5 — Example of dilatometry curves obtained by the laboratory-built dilatometer (cooling only) and by the commercial dilatometer. The transformation temperatures of 480°, 395°, 365,° and 360°C for the different samples are indicated by the dotted lines.

The bainite start curve occurs at slightly higher values for $\Delta t_{8/5}$ and lower temperatures than the curve in the X70 CCT diagram in Ref. 12. Our result indicates that the hardenability of the tested material is higher than that of the material investigated in Ref. 12, which in turn may be attributed to the slight difference in chemical composition between the two steels.

It is believed that the sample geometry-dependent finish temperatures can be explained by a relatively large radial temperature gradient in the cylindrical specimens with the lower temperature at the surface during cooling. Since the measured dilatation is plotted vs. surface temperature, a too

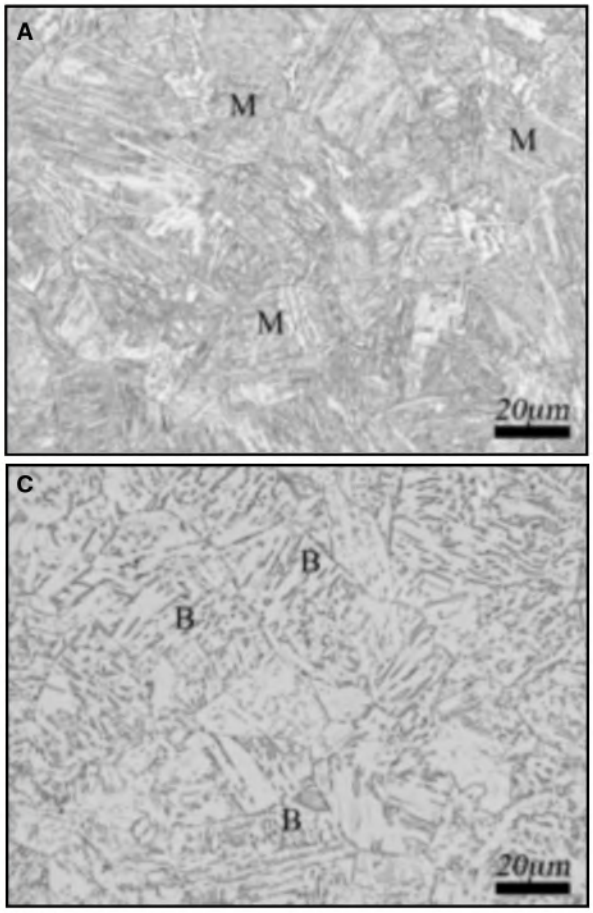

Fig. 6 — Microstructure in samples with 3-mm diameter subjected to thermal cycles in the dilatometry tests. A — T_p = 1215°C, $\Delta t_{8/5}$ = 1.4 s; B — T_p = 1197°C, $\Delta t_{8/5}$ = 7.3 s; C — T_p = 1217°C, $\Delta t_{8/5}$ = 23.5s.

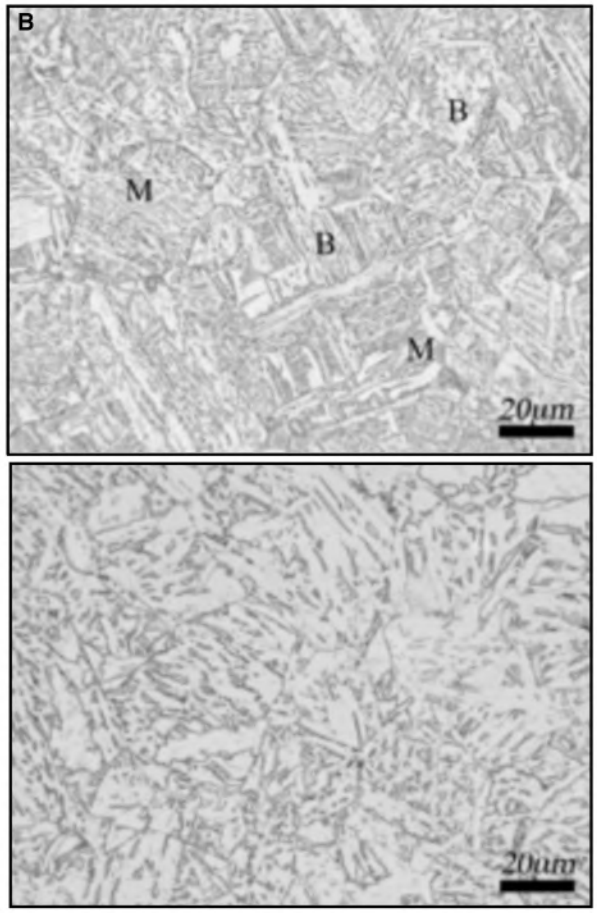

Fig. 7 — Microstructure in a dilatometry sample with 10-mm diameter subjected to a thermal cycle with T_p = 1200°C and $\Delta t_{8/5}$ = 107.2 s.

low value of the latter compared to the average temperature in the sample would result in an artificially low value for the transformation. And the inaccuracy will increase with sample size and cooling rate due to the corresponding increase in temperature gradient. This assumption is supported by the findings of Alexandrov et al. (Ref. 21) who suggested that the temperature gradient in the sample cross section was a possible reason for the delay in the dilatometer response in experiments comparing single-sensor differential thermal analysis to dilatometry.

Relatively large longitudinal temperature gradients exist also in the square samples. Walsh et al. (Ref. 22) examined the magnitude of such gradients as well as the major factors affecting the gradients in an experimental setup similar to that used in the commercial dilatometer in the current investigation. The specimen maximum temperature of about 1200°C was obtained in the mid position between the water-cooled copper clamps; the clamped ends being kept at about 4°C. It is believed that the lower transformation finish tem-

Table 2 — Results from the Dilatometry Measurements

Sample geometry	Tp [°C]	$\Delta t_{8/5}$ [s]	Ts [°C]	Tf [°C]	Microstructure [vol-%.]			Hardness
					M	B	Std. Dev.	[HV10]
Diameter 3 mm	1215	1.4	437	295	100	0	0.0	340
Diameter 3 mm	1197	7.3	530	395	62	38	3.7	277
Diameter 3 mm	1217	23.5	590	480	0	100	0.0	212
Diameter 10 mm	1233	5.5	540	365	57	43	4.4	268
Diameter 10 mm	1230	9.8	590	410	28	72	5.0	252
Diameter 10 mm	1250	21.7	590	480	0	100	0.0	225
Diameter 10 mm	1200	107.2	630	490	0	100	0.0	202
Square, 10 × 10 mm	1204	6.5	560	360	66	34	4.5	294
Square, 10 × 10 mm	1210	10.2	585	410	46	54	5.1	264
Square, 10 × 10 mm	1206	22.6	610	480	0	100	0.0	231
Square, 10 × 10 mm	1217	109.4	620	530	0	100	0.0	209

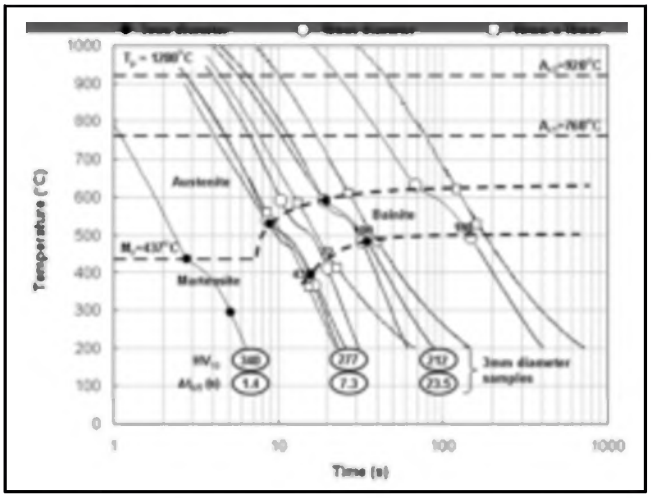

Fig. 8 — CCT diagram for the X70 steel obtained after cooling from 1200°C using different cooling rates.

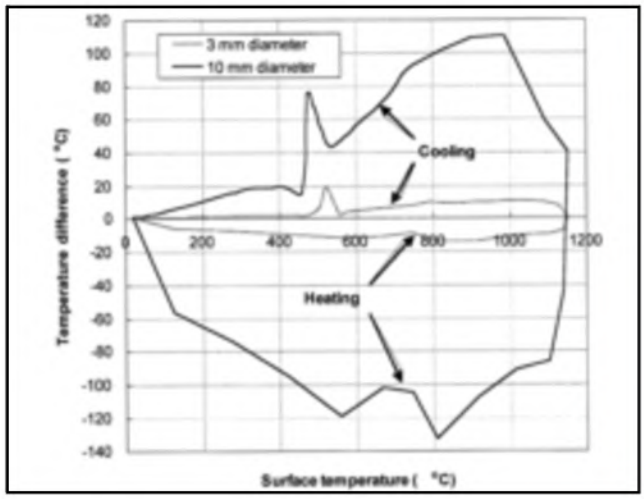

Fig. 9 — Computed temperature differences ($T_{center} - T_{surface}$) between the sample center and surface as a function of temperature during heating and cooling. The calculated results apply for cylindrical samples of 3- and 10-mm diameter subjected to a thermal cycle with T_p = 1200°C and $\Delta t_{8/5}$ = 5.5 s.

peratures occurred as a result of a measured surface temperature during cooling being lower than the average temperature in the sample cross section. The transformation finish will thus apparently occur at a temperature lower than the average temperature in the sample cross section.

The existence of thermal gradients within the cylindrical samples was verified by the previously mentioned *WeldsimS* simulation. Figure 9 displays the temperature difference between the center and the surface of the samples as a function of temperature during heating and cooling. It is seen that there is a relatively large temperature difference for the 10-mm-diameter sample, while this difference is much smaller for the 3-mm-diameter sample. Note also the impact of phase transformation during cooling on the temperature gradients for the sample of 10-mm diameter in the temperature interval 400°–550°C. During cooling, the ferritic transformation starts at the surface of the sample and as transformation heat is removed, the temperature difference between surface and center decreases. When the transformation is finished in the surface region; the temperature difference between surface and center increases due to the removal of transformation heat in the sample center. When transformation is complete in the whole sample cross section, temperature differences decrease again. It should also be mentioned that temperature gradients within the sample may induce plastic deformations, which in turn may affect the phase transformation during cooling (Ref. 23).

Conclusions

A CCT diagram valid for the HAZ in welding operations with relatively rapid heating to about 200°C for X70 pipeline steel with composition given in Table 1 has been established by means of dilatometry and metallographic analyses. The M_s, A_{c1}, and A_{c3} temperatures were found to be 437°, 760°, and 920°C, respectively. At cooling times $\Delta t_{8/5}$ of below 10 s, the microstructure of the samples consists of a mixture of bainite and martensite, with formation of a fully martensitic microstructure at the shortest cooling time. Cooling times above 20 s resulted in the formation of 100% bainitic microstructure. Even at cooling times $\Delta t_{8/5}$ as high as 109 s, 100% bainite was formed. Also, the linear thermal expansion coefficients for austenite and bainite were measured. The values are 2.09×10^{-5} and 1.29×10^{-5} K^{-1}, respectively. The importance of using relatively small dilatometry samples in order to minimize the inaccuracy associated with the temperature gradients has been substantiated by means of mathematical modeling showing that cylindrical samples of 20-mm length and 3-mm diameter are sufficiently small.

Acknowledgments

The authors thank Hallvard Fjær at the Institute for Energy Technology, Norway, for carrying out the heat transfer calculations. Financial support from the Norwegian Research Council through the RESIA STORFORSK Project (Project No. 167397/V30) is gratefully acknowledged.

Appendix

Analysis of Thermal Gradients during the Dilatometry Experiments

In order to assess the thermal gradients in the samples during the dilatometry experiments, the FEM software *WeldsimS* was employed (Refs. 5, 16). In this model, the effect of the phase transformations on the heat transfer is taken into account. The heat transfer and phase transformation modules of *WeldsimS* are described in more detail in Refs. 5 and 16. Brief descriptions of both models as well as the conditions for the heat transfer analysis carried in the present work are outlined below.

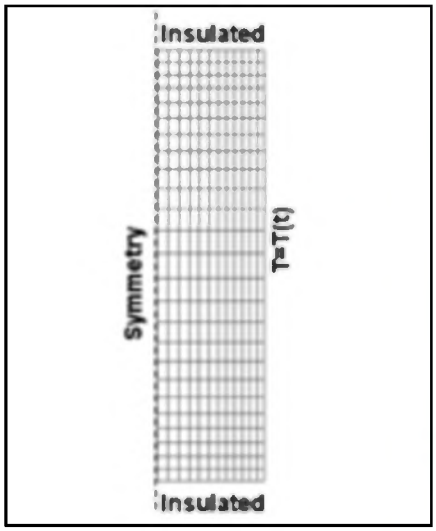

Fig. 10 — FEM mesh employed in the heat transfer analysis of dilatometry experiment with the 10-mm samples as well as boundary conditions employed in the simulations.

Model Description

In *WeldsimS*, the metallurgical state of steel is characterized by the fractions p_i of its different constituents (e.g., austenite, ferrite, pearlite, bainite, and martensite) satisfying the condition

$$\sum p_i = 1 \qquad (1)$$

By assuming linear mixing laws, and by defining an enthalpy H_i for each phase by

$$H_i(T) = H_i^0 + \int_{T_0}^{T} c_{p,i}(T)\,dT \quad (2)$$

The equation for the transient heat transfer can be written as

$$\sum_i \rho_i p_i c_{p,i} \dot{T} + \sum_i \rho_i \dot{p}_i H_i = \nabla \cdot \left(\sum_i p_i \lambda_i \nabla T \right) + Q \quad (3)$$

where ρ_i, λ_i, $c_{p,i}$, and T denote, respectively the density, thermal conductivity, specific heat for phase i, and the temperature. H^0_i is the enthalpy of phase i at the reference temperature T_0 and Q is the internal heat source. T and p_i in Equation 3 are derivatives with respect to time. Note that the second term on the left side of Equation 3 represents the transformation heat associated with the phase change.

Solving Equation 3 requires the knowledge of the phase proportions p_i. For this purpose, the anisothermal transformation kinetics model by Leblond and Devaux (Ref. 24), which has previously been implemented in *WeldsimS*, is employed. Up to five metallurgical phases (austenite, ferrite, pearlite, bainite, and martensite) can be taken into account in *WeldsimS*. To illustrate the modeling equations in the case of two phases (denoted 1 and 2), one has to distinguish between the $1 \rightarrow 2$ ($p_1 > 0$) and the $2 \rightarrow 1$ ($p_2 > 0$) transformations. For each case, the rate of transformation is given by

$$\dot{p}_1 = \left(\frac{p_{21}^{eq}(T) - p_1}{\tau_{21}(T)} \right) \cdot f_{21}(\dot{T}) \quad (2 \rightarrow 1 \text{ transformation}) \quad (4)$$

$$\dot{p}_2 = \left(\frac{p_{12}^{eq}(T) - p_2}{\tau_{12}(T)} \right) \cdot f_{12}(\dot{T}) \quad (1 \rightarrow 2 \text{ transformation}) \quad (5)$$

where p_1 and p_2 denote the fraction of phase 1 and 2, respectively, with $p_1 + p_2 = 1$. p^{eq}_{21} (p^{eq}_{12}) is the value of p_1 (p_2) at equilibrium for a given temperature, and $\tau_{21}(\tau_{12})$ is the characteristic time for the transformation $2 \rightarrow 1$ ($1 \rightarrow 2$). The functions $f_{21}(\dot{T})$, and $f_{12}(\dot{T})$ allow for taking into account the effect of the cooling rate. All these parameters are obtained by fitting the phase fractions from various heating/cooling curves to hit correctly the A_{C1}/A_{C3} (during heating) and the start/end temperatures for the ferritic transformations shown in CCT diagrams (during cooling).

Application to X70 Steel

To obtain the modeling results of Fig. 9, 2-D axis-symmetry models have been established using cylindrical geometries with the same radii and heights as the samples employed in the dilatometry experiments (i.e., 5.0×20.0 mm^2 and 1.5×20.0 mm^2). Figure 10 shows the mesh employed in the thermal analysis as well as the thermal boundary conditions. Due to symmetry reason, the computation domain corresponds to half of the sample. The mesh is made of 300 elements and 338 nodes. Thermophysical data in the modelling were taken from the literature and are the same as those applied in Ref. 16. Parameters used for the phase transformation model are based on the work of Ref. 5 and were extracted using the CCT diagram of Hulka et al. (Ref. 12), which is obtained for a steel similar to the X70 material studied in the present work.

As seen in Fig. 10, a time-dependent temperature is imposed as a thermal boundary condition on the vertical surface of the cylinders, while the top and bottom surfaces are insulated. For both geometries, the imposed temperature as a function of time corresponds to the surface measurements for the thermal cycle with T_p = 1200°C and $\Delta t_{8/5}$ = 5.5 s. For this cycle, the peak temperature is reached after approximately 10 s of heating time.

References

1. Taljat, B., Radhakrishnan, B., and Zacharia, T. 1998. Numerical analysis of GTA welding process with emphasis on post-solidification phase transformation effects on residual stresses. *Materials Science and Engineering* A, (246): 45–54.

2. Ferro, P., Porzner, H., Tiziani, A., and Bonollo, F. 2006. The influence of phase transformations on residual stress induced by the welding process — 3D and 2D numerical models. *Modelling and Simulation in Materials Science and Engineering*, (14): 117–136.

3. Brown, T. B., Dauda, T. A., Truman, C. E., Smith, D. J., Memhard, D., and Pfeiffer, W. 2006. Prediction and measurements of residual stress in repair welds in plates. *International Journal of Pressure Vessels and Piping*, (83): 809–818.

4. Deng, D., and Murakawa, H. 2006. Prediction of welding residual stress in multi-pass butt-welded modified 9Cr-1Mo steel pipe considering phase transformation effects. *Computational Materials Science*, (37): 209–219.

5. Aarbogh, H. M., M'Hamdi, M., Mo, A., and Fjær, H. G. 2007. A simplified method for establishing constitutive equations and flow stress data for welding stress modelling. Accepted for publication in the *Science and Technology of Welding and Joining*.

6. Garcia de Andres, C., Caballero, F., Capdevila, G. C., and Alvarez, L. F. 2002. Application of dilatometric analysis to the study of solid-solid phase transformations in steels. *Materials Characterization*, (48): 101–111.

7. Reed, R. C., Akbay, T., Shen, Z., Robinson, J. M., and Root, J. H. 1988. Determination of reaustenitisation kinetics in a Fe-0.4C steel using dilatometry and neutron diffraction. *Materials Science and Engineering* A, (256): 152–165.

8. De Cock, T., Capdevila, C., Caballero, F. G., and Garcia de Andres, C. 2006. Interpretation of a dilatometric anomaly previous to the ferrite-to-austenite transformation in a low carbon steel. *Scripta Materialia*, (54): 949–954.

9. Leblond, J. B., Mottet, G., and Devaux, J. C. 1986. A theoretical and numerical approach to the plastic behaviour of steels during phase transformations — I. Derivation of general relations. *Journal of Mechanical Physics of Solids*, (34): 395–409.

10. Zhang, M., Li, L., Fu, R. Y., Krizan, D., and De Cooman. B. C. 2006. Continuous cooling transformation diagrams and properties of micro-alloyed TRIP steels. *Materials Science and Engineering* A, (438–440): 296–299.

11. Zhao, M. C., Yang, K., Xiao, F. R., and Shan, Y. Y. 2003. Continuous cooling transformation of undeformed and deformed low carbon pipeline steels. *Materials Science and Engineering* A, (355): 126–136.

12. Hulka, K., Gray, J. M., and Heisterkamp, F. 1990. Niobium Technical Report NbTR 16/90, CBMM, Sao Paulo, Brazil.

13. *HBM Mess- und Systemtechnik Prüfprotokoll Wegaufnehmer*. 1998. Ident.-Nr. 022440007.

14. API Spec. 5L, Specification for line pipe, Rev. 44, 2007.

15. Onsøien, M. I., Gundersen, Ø., and Akselsen, O. M. 1997. Upgrading of Smitweld TCS 1405 weld simulator, Sintef report STF24 A97401, Trondheim, Norway.

16. Fjær, H. G., Liu, J., M'Hamdi, M., and Lindholm. D. 2007. On the use of residual stresses from welding simulations in failure assessment analysis for steel structures. H. Cerjak, H. K. D. H. Bhadeshia, and E. Kozeschnik, editors, *Mathematical Modelling of Weld Phenomena* 8, 96 –979.

17. Kluken, A. O., Onsøien, M. I., Akselsen, O. M., and Rørvik, G. 1991. Mechanical properties of high heat input deposited weld metals. *Joining Sciences*, (1): 14–22.

18. Krauss, G. 1993. Steels: *Heat Treatment and Processing Principles*. ASM International, Materials Park, Ohio, 169–177.

19. Andrews, K. W. 1965. Empirical formulae for the calculation of some transformation temperatures. *Journal of the Iron and Steel Institute*, (203): 721–727.

20. Takahashi, M. 1992. Reaustenitization from bainite in steels. PhD thesis, University of Cambridge, Cambridge, UK.

21. Alexandrov, B. T., and Lippold, J. C. 2007. Single sensor differential thermal analysis of phase transformations and structural changes during welding and postweld heat treatment. *Welding in the World*, 51 (11/12): 48–59.

22. Walsh, D. W., Cieslak, M. J., and Savage, W. F. 1986. Temperature measurements in resistance heated specimens: Longitudinal gradients. *Welding Journal*. 65 (7): 184-s to 192-s.

23. Bhadeshia, H. K.D. H. 2004. Developments in martensitic and bainitic steels: role of the shape deformation. *Materials Science and Engineering* A, (378): 34–39.

24. Leblond, L. B., and Devaux, J. 1984. A new kinetic model for anisothermal metallurgical transformations in steels including effect of austenite grain size, *Acta Metall*, (32): 137–146.